universe

MDPI

Article

Search for Double Beta Decay of ^{106}Cd with an Enriched $^{106}CdWO_4$ Crystal Scintillator in Coincidence with $CdWO_4$ Scintillation Counters

Pierluigi Belli [1,2], R. Bernabei [1,2,*], V.B. Brudanin [3], F. Cappella [4,5], V. Caracciolo [1,2,6], R. Cerulli [1,2], F. A. Danevich [7], Antonella Incicchitti [4,5], D.V. Kasperovych [7], V.R. Klavdiienko [7], V.V. Kobychev [7], Vittorio Merlo [1,2], O.G. Polischuk [7], V.I. Tretyak [7] and M.M. Zarytskyy [7]

1. INFN, Sezione di Roma "Tor Vergata", I-00133 Rome, Italy; pierluigi.belli@roma2.infn.it (P.B.); vincenzo.caracciolo@roma2.infn.it (V.C.); riccardo.cerulli@roma2.infn.it (R.C.); vittorio.merlo@roma2.infn.it (V.M.)
2. Dipartimento di Fisica, Università di Roma "Tor Vergata", I-00133 Rome, Italy
3. Joint Institute for Nuclear Research, 141980 Dubna, Russia; brudanin@jinr.ru
4. INFN, Sezione Roma "La Sapienza", I-00185 Rome, Italy; fabio.cappella@roma1.infn.it (F.C.); antonella.incicchitti@roma1.infn.it (A.I.)
5. Dipartimento di Fisica, Università di Roma "La Sapienza", I-00185 Rome, Italy
6. INFN, Laboratori Nazionali del Gran Sasso, 67100 Assergi (AQ), Italy
7. Institute for Nuclear Research of NASU, 03028 Kyiv, Ukraine; danevich@kinr.kiev.ua (F.A.D.); casper.phys@gmail.com (D.V.K.); klavdiienko.volodymyr@gmail.com (V.R.K.); kobychev@kinr.kiev.ua (V.V.K.); polischuk@kinr.kiev.ua (O.G.P.); tretyak@kinr.kiev.ua (V.I.T.); zaritsky96@gmail.com (M.M.Z.)

* Correspondence: rita.bernabei@roma2.infn.it

Received: 3 September 2020; Accepted: 12 October 2020; Published: 16 October 2020

check for updates

Abstract: Studies on double beta decay processes in ^{106}Cd were performed by using a cadmium tungstate scintillator enriched in ^{106}Cd at 66% ($^{106}CdWO_4$) with two $CdWO_4$ scintillation counters (with natural Cd composition). No effect was observed in the data that accumulated over 26,033 h. New improved half-life limits were set on the different channels and modes of the ^{106}Cd double beta decay at level of lim $T_{1/2} \sim 10^{20} - 10^{22}$ yr. The limit for the two neutrino electron capture with positron emission in ^{106}Cd to the ground state of ^{106}Pd, $T_{1/2}^{2\nu EC\beta^+} \geq 2.1 \times 10^{21}$ yr, was set by the analysis of the $^{106}CdWO_4$ data in coincidence with the energy release 511 keV in both $CdWO_4$ counters. The sensitivity approaches the theoretical predictions for the decay half-life that are in the range $T_{1/2} \sim 10^{21} - 10^{22}$ yr. The resonant neutrinoless double-electron capture to the 2718 keV excited state of ^{106}Pd is restricted at the level of $T_{1/2}^{0\nu 2K} \geq 2.9 \times 10^{21}$ yr.

Keywords: double beta decay; ^{106}Cd; scintillation detector; low background experiment

1. Introduction

Observations of the neutrino oscillations suggest that the neutrinos are massive, which calls for an extension of the Standard Model of particles and fields (SM). However, oscillation experiments cannot determine the neutrino mass and the neutrino mass hierarchy. One of the most promising tools for determining the absolute neutrino mass scale and the neutrino mass hierarchy, the nature of the neutrino (Dirac or Majorana particle?), in order to check the lepton number conservation is double beta (2β) decay of atomic nuclei, a process in which two electrons (or positrons) are simultaneously emitted and nuclear charge changes by two units: (A,Z)→(A,Z±2) [1–3]. The neutrinoless mode of the decay ($0\nu2\beta$) violates the lepton number conservation law and it is possible if the neutrinos are Majorana particles (particle is equal to its antiparticle). Being a process beyond the SM, the $0\nu2\beta$ decay has the potential to test the SM [4–6]. Moreover, the Majorana nature of the neutrino might shed light on the Universe baryon asymmetry problem [7,8].

The two-neutrino 2β decay ($2\nu2\beta$) is a radioactive process that is allowed in the SM with the longest half-lives ever observed: 10^{18}–10^{24} yr. The $2\nu2\beta^-$ decay mode has been detected in several nuclides [9]. The $0\nu2\beta$ decay is not observed. The most sensitive $2\beta^-$-decay experiments quote half-life limits at level of $T_{1/2} > (10^{24} - 10^{26})$ yr, which correspond to Majorana neutrino mass limits in the range $\langle m_\nu \rangle < (0.1 - 0.7)$ eV. Probing the inverted hierarchy region of the neutrino mass requires improved sensitivities of $2\beta^-$ experiments at the level of $\langle m_\nu \rangle \sim (0.02 - 0.05)$ eV (i.e., half-life sensitivity in the range: $T_{1/2} \sim 10^{27} - 10^{28}$ yr).

The sensitivity of the experiments in the search for "double beta plus" processes: double electron capture (2EC), electron capture with positron emission ($EC\beta^+$), and double positron decay ($2\beta^+$) is substantially lower, while the physical lepton-number violating mechanisms of the neutrinoless 2EC, $EC\beta^+$ and $2\beta^+$ processes are considered to be essentially the same as for the decay with electrons emission. At the same time, there is a motivation to search for the $0\nu EC\beta^+$ and $0\nu2\beta^+$ decays owing to the potential to clarify the possible contribution of the right-handed currents to the $0\nu2\beta^-$ decay rate [10], and an interesting possibility of a resonant 0ν2EC process [11–14].

As for the allowed two-neutrino mode of the double beta plus decay, there are claims of positive results (indication) for the 2ν2EC radioactivity of three nuclides. The 2ν2EC decay of ^{130}Ba was claimed in two geochemical experiments where anomaly in the isotopic concentrations of daughter xenon traces in old barite ($BaSO_4$) minerals was interpreted as the sought effect with the half-life $T_{1/2} = (2.16 \pm 0.52) \times 10^{21}$ yr [15], and with $T_{1/2} = (6.0 \pm 1.1) \times 10^{20}$ yr in [16]. In the analysis [17], the disagreement was explained by a possible cosmogenic contribution with a conclusion that the result of [15] is a more reliable one. An indication on the 2ν2EC process in ^{78}Kr with the half-life $T_{1/2} = 9.2^{+5.7}_{-2.9} \times 10^{21}$ yr was obtained with a proportional counter with a volume of 49 lt filled by gas enriched in ^{78}Kr to 99.81% [18]. The value was then updated to $1.9^{+1.3}_{-0.8} \times 10^{22}$ yr in [19]. Recently, a detection of the 2ν2EC of ^{124}Xe with the half-life $(1.8 \pm 0.5) \times 10^{22}$ yr was claimed in [20]. However, the indications of ^{130}Ba 2EC decay should be confirmed in direct counting experiments, while the results for ^{78}Kr and ^{124}Xe need to be confirmed with bigger statistics and very stable experiments. Other allowed 2ν decay channels with decrease of the nuclear charge by two units, $2\nu EC\beta^+$ and $2\nu2\beta^+$, are not observed yet.

The nuclide ^{106}Cd is one of the most appealing candidates to search for 2EC, $EC\beta^+$, and $2\beta^+$ decays with a long history of studies (a review of the previous investigations reader can find in Ref. [21]). The interest to ^{106}Cd can be explained by one of the biggest decay energy $Q_{2\beta} = 2775.39(10)$ keV [22], comparatively high isotopic abundance $\delta = 1.245(22)\%$ [23], and possibility of gas centrifugation for enrichment, existing technologies of cadmium purification, the availability of Cd-containing detectors to realize calorimetric experiments with a high detection efficiency.

Presently, there are three running experiments searching for the double beta decay of ^{106}Cd: COBRA, TGV-2, and the present one.

The COBRA collaboration utilizes CdZnTe semiconductor detectors at the Gran Sasso underground laboratory (Laboratori Nazionali del Gran Sasso, LNGS). The experiment started with one $Cd_{0.9}Zn_{0.1}Te$ detector with mass of $\simeq$3 g, and one CdTe detector ($\simeq$6 g) [24]. CdZnTe detectors are used in the current stage of the experiment [25,26]. The measurements resulted in the half-life limits for several channels of ^{106}Cd double beta decay at the level of $\sim 10^{18}$ yr.

The main goal of the TGV-2 experiment, which is located at the Modane underground laboratory, is the search for 2ν2EC decay of ^{106}Cd (a decay channel expected to be the fastest one) with the help of 32 planar HPGe detectors with a total sensitive volume ≈ 400 cm^3. In the first stage of the experiment, foils of cadmium enriched in ^{106}Cd to (60–75)% were used [27–29]; now, 23.2 g of cadmium sample enriched in ^{106}Cd to 99.57% are installed in the set-up [30]. The experiment gives the strongest limit on the 2ν2EC decay: $T_{1/2} > 4.7 \times 10^{20}$ yr. For other decay modes and channels, the sensitivity is at level of 10^{20} yr [31].

A cadmium tungstate crystal scintillator from cadmium enriched in ^{106}Cd to 66% (^{106}CdWO$_4$) was developed in 2010 [32]. The experiments with that detector are carried out at the LNGS in the DAMA/CRYS, DAMA/R&D set-ups, and in an ultra-low background GeMulti HPGe γ spectrometer of the STELLA (SubTErranean Low Level Assay) facility [33] at the LNGS. The first stage of the experiment with the ^{106}CdWO$_4$ detector gave the half-life limits on 2β processes in ^{106}Cd at level of $\sim 10^{20}$ yr [21]. In the second stage, the ^{106}CdWO$_4$ scintillator was installed between four HPGe detectors (with volume $\simeq 225$ cm^3 each) of the GeMulti HPGe γ spectrometer to detect γ quanta expected in the most of the ^{106}Cd decay channels, including the annihilation γ's emitted in decay modes with positron(s) emission (a simplified decay scheme of ^{106}Cd is presented in Figure 1). The experiment improved the ^{106}Cd half-life limits to the level of $T_{1/2} \geq (10^{20} - 10^{21})$ yr [34]. In the third stage, described in the present report, the ^{106}CdWO$_4$ detector was running in coincidence (anti-coincidence) with two large volume CdWO$_4$ crystal scintillators in a close geometry in order to increase the detection efficiency to γ quanta expected to be emitted from the ^{106}CdWO$_4$ crystal in the double beta decay processes in ^{106}Cd. Preliminary results of the experiment stage were reported in [35].

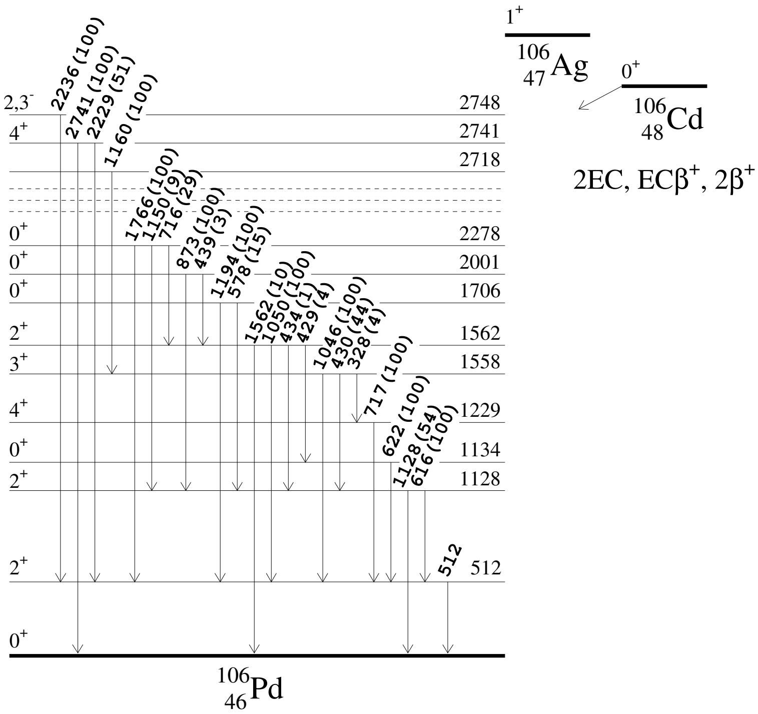

Figure 1. Simplified decay scheme of ^{106}Cd [36] (levels with energies in the energy interval (2283–2714) keV are omitted). The energies of the excited levels are in keV. Relative intensities of γ quanta are given in parentheses.

2. The Experiment

The ^{106}CdWO$_4$ crystal scintillator of roughly cylindrical shape (approximate sizes ⌀27 mm × 50 mm, mass 215.4 g) was viewed by a three inches low radioactive photo-multiplier tube (PMT) Hamamatsu R6233MOD through a lead tungstate (PbWO$_4$) crystal light-guide (⌀40 mm × 83 mm). The PbWO$_4$ crystal has been developed from the highly purified [37] archaeological lead [38]. Two CdWO$_4$ crystal scintillators ⌀70 mm × 38 mm include a cylindrical cut-out to house the ^{106}CdWO$_4$ crystal. They were viewed by two three-inch low radioactive PMTs EMI9265B53/FL through light-guides glued in two parts: low radioactive quartz (⌀66 mm × 100 mm, close to the CdWO$_4$ scintillators) and optical quality polystyrene (⌀66 mm × 100 mm). Figure 2 shows a schematic of the set-up. The detector system was surrounded by four high purity copper bricks (referred hereinafter as "internal copper") and by layers of high purity copper (11 cm, hereinafter referred as "external copper"), low radioactive lead (10 cm), cadmium (2 mm), and polyethylene (10 cm) in order to reduce the external background. The inner volume of the set-up with the detector system was continuously flushed by high-purity nitrogen gas to remove environmental radon. The grade of the high-purity N_2 gas is at least 5.5, for what concerns the presence of other possible gases. However, the possible presence in trace of Radon gas in the Nitrogen atmosphere inside the copper box, housing the detector, has been checked with another set-up, by searching for the double coincidences of the γ-rays (609 and 1120 keV) from ^{214}Bi Radon daughter. The obtained upper limit on the possible Radon concentration in the high-purity Nitrogen atmosphere has been measured to be: $<5.8 \times 10^{-2}$ Bq/m^3 (90% C.L.) [39]. Figure 3 shows photographs of the detector system.

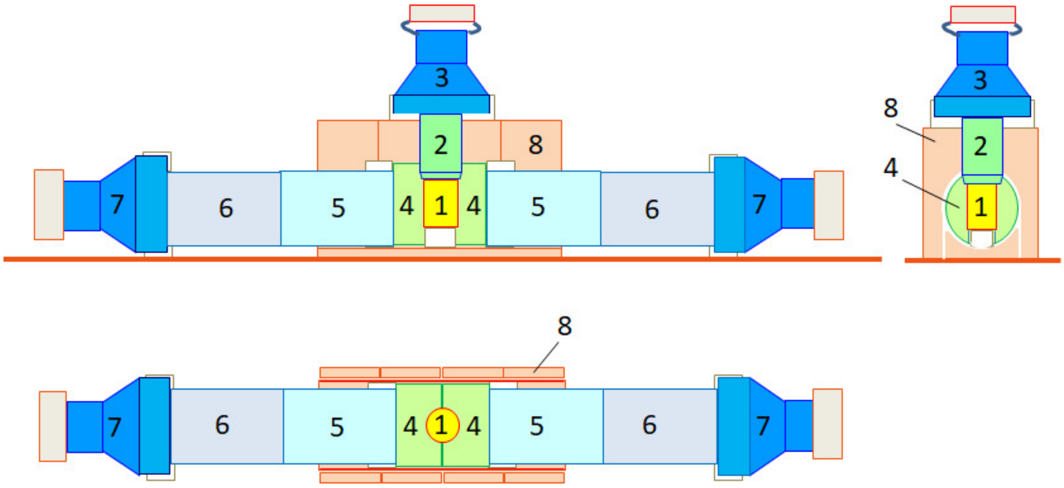

Figure 2. Schematic of the experimental set-up with the ^{106}CdWO$_4$ scintillation detector. ^{106}CdWO$_4$ crystal scintillator (1) is viewed through PbWO$_4$ light-guide (2) by photo-multiplier tube (3). Two CdWO$_4$ crystal scintillators (4) are viewed through light-guides glued from quartz (5) and polystyrene (6) by photo-multiplier tubes (7). The detector system was surrounded by passive shield made from copper, lead, polyethylene, and cadmium (not shown). Only part of the copper details (8, "internal copper"), used to reduce the direct hits of the detectors by γ quanta from the PMTs, are shown.

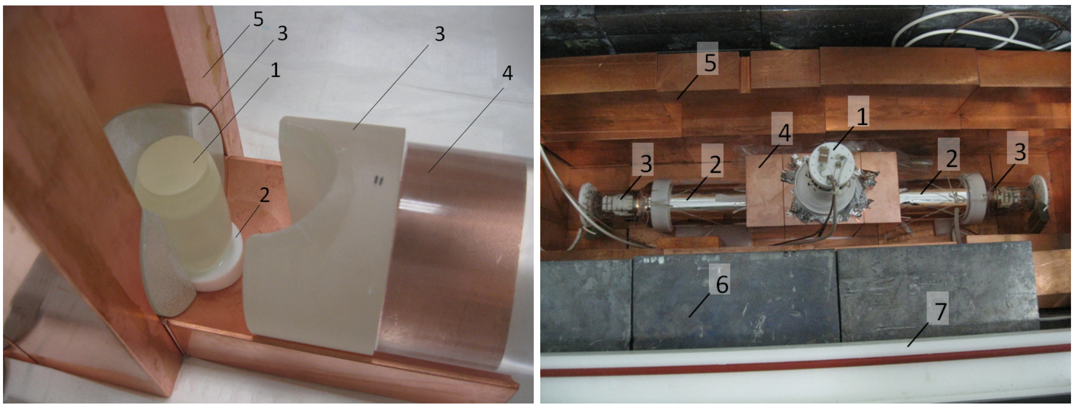

Figure 3. Left photograph: the ^{106}CdWO$_4$ crystal scintillator (1), Teflon support of the ^{106}CdWO$_4$ crystal (2), CdWO$_4$ crystal scintillators (3), quartz light-guide (4), "internal copper" brick (5). Right photograph: the detector system installed in the passive shield: PMT of the ^{106}CdWO$_4$ detector (1), light-guides of the CdWO$_4$ counters wrapped by reflecting foil (2), PMT of the CdWO$_4$ counters (3), "internal copper" bricks (4), "external copper" bricks (5), lead bricks (6), and polyethylene shield (7). The copper, lead and polyethylene shields are not completed.

An event-by-event data acquisition system that is based on a 100 MS/s 14 bit transient digitizer (DT5724 by CAEN) recorded the amplitude, the arrival time, and the pulse shape of each event. To reduce the data volume due to presence in the $^{106}CdWO_4$ crystal of ^{113}Cd and ^{113m}Cd β active nuclides [21,32], the energy threshold for the set-up was set at level of ≈510 keV for the anti-coincidence mode, while the energy threshold of the $^{106}CdWO_4$ detector in the coincidence with the $CdWO_4$ counters was ≈200 keV. The energy thresholds of the $CdWO_4$ counters were ≈70 keV. The energy scale and energy resolution of the detectors were measured with ^{22}Na, ^{60}Co, ^{133}Ba, ^{137}Cs, and ^{228}Th γ sources at the beginning, in the middle and end of the experiment.

The energy resolution of the $^{106}CdWO_4$ detector for the total exposure can be described by the function FWHM $= 6.85 \times \sqrt{E_\gamma}$, where FWHM (full width at half maximum) and E_γ are given in keV. The poor energy resolution of the enriched detector (despite excellent optical properties of the material [32]) is caused by the elongated shape of the enriched scintillator that results in a rather low and non-uniform light collection, and by the using of not perfectly transparent $PbWO_4$ crystal light-guide. The performance of the $CdWO_4$ counters is substantially better. The energy spectra that were accumulated by one of the counters with ^{22}Na, ^{60}Co and ^{228}Th γ sources are presented in Figure 4. The energy resolution of the counters was estimated by using the results of the three energy calibration campaigns as FWHM $= a \times \sqrt{E_\gamma}$ with the coefficient a equal to 2.97 and 3.13 for the two detectors. The resolution formulas also take into account energy scale shifts during the data taking over the experiment.

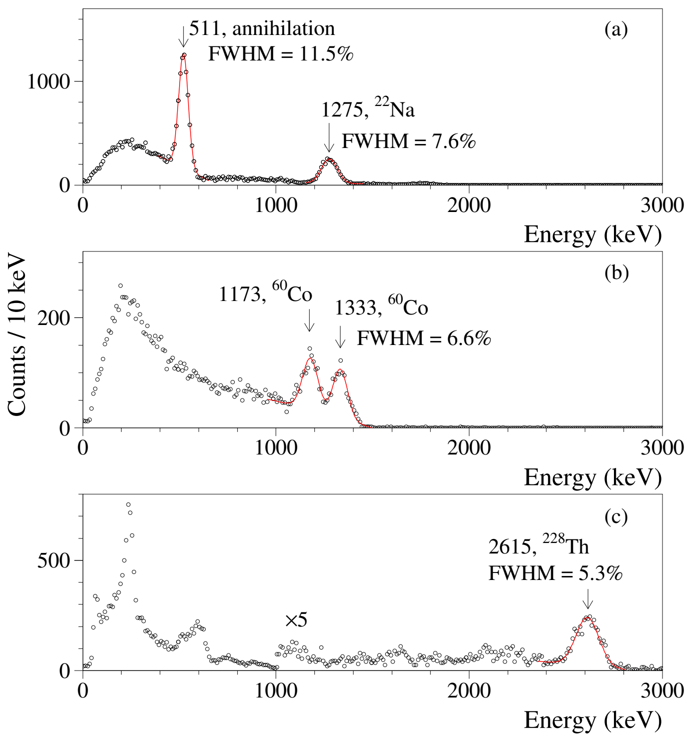

Figure 4. Energy spectra of ^{22}Na (**a**), ^{60}Co (**b**) and ^{228}Th (**c**) γ quanta measured by one of the $CdWO_4$ detectors. Fits of intensive γ peaks by Gaussian functions are shown by solid lines. Energies of γ quanta are in keV.

The energy spectra of ^{22}Na source were simulated by the EGSnrc code [40]. The data measured with ^{22}Na source without coincidence selection and in coincidence with energy 511 keV in at least one of the $CdWO_4$ counters is compared with the simulated distribution in Figure 5. The experimental data are in reasonable agreement with the results of simulations.

The inset of Figure 5 shows a distribution of the $^{106}CdWO_4$ detector pulses start positions relative to the $CdWO_4$ signals with energy 511 keV. The time resolution of the detector system is rather high (the standard deviation of the distribution is 16 ns) due to the fast rise time of the $CdWO_4$ scintillation pulses.

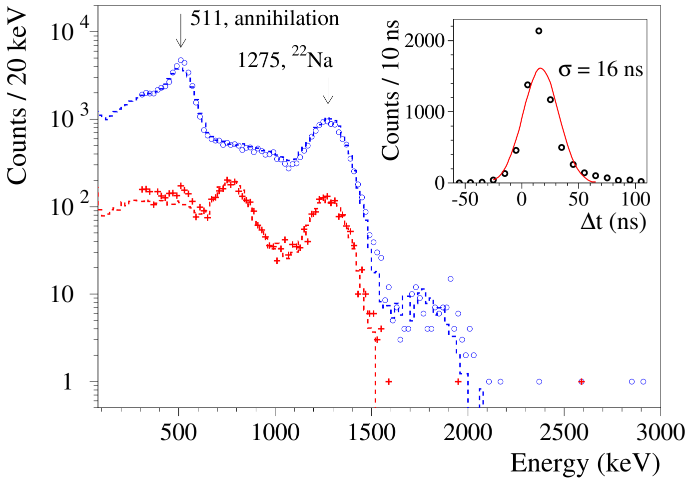

Figure 5. Energy spectra of ^{22}Na γ quanta measured by the $^{106}CdWO_4$ detector: with no coincidence cuts (blue circles) and in coincidence with energy 511 keV in at least one of the $CdWO_4$ counters (red crosses). The data simulated by using the EGSnrc Monte Carlo code are drawn by dashed lines. (Inset) Distribution of the $^{106}CdWO_4$ detector pulses start positions relative to the $CdWO_4$ signals with the energy 511 keV.

3. Results and Discussion

3.1. Backgrounds Reduction and Model of the Backgrounds

The difference in $CdWO_4$ scintillation pulse shape for β particles (γ quanta) and α particles can be used in order to suppress the background caused by α radioactive contamination of the detector due to the residual contamination in ^{232}Th and ^{238}U with their daughters. The mean time method was applied to the data in order to discriminate signals of different origin by pulse shape. For each signal $f(t)$, the numerical characteristic of its shape (mean time, ζ) was defined using the following equation:

$$\zeta = \sum f(t_k) \cdot t_k / \sum f(t_k), \quad (1)$$

where the sum is over the time channels k, starting from the origin of signal up to 35 μs; $f(t_k)$ is the digitized amplitude (at the time t_k) of a given signal. The energy dependence of the parameter ζ and its standard deviation (the distributions of ζ for β particles (γ quanta) and α particles are well described by a Gaussian function) was determined by using the data of the calibration measurements with ^{228}Th gamma source. The obtained parameters were then used to discriminate β (γ) events from α events in the data of the low-background experiment. We refer the reader to our previous works [21,34], where the pulse-shape discrimination (PSD) method was described in detail.

By using the PSD, the α events were statistically separated from $\gamma(\beta)$ events. In addition the method discarded from the data events of the ^{212}Bi – ^{212}Po sub-chain from the ^{232}Th family (due to the short decay time of ^{212}Po $\approx$ 0.3 μs these decays are treated by the data acquisition system as a single event), PMT noise, pile-ups of signals in the $^{106}CdWO_4$ detector, $^{106}CdWO_4$ plus $PbWO_4$ events, etc. Figure 6 shows the results of the PSD method application to the background data gathered for 26,033 h in the low-background set-up. The mean time method reduced the background mainly in the energy region (800–1300) keV (by a factor $\sim$1.6), where α events of the ^{232}Th and ^{238}U with their daughters are expected.

Further reduction of the background counting rate (by a factor $\sim$1.3 in the energy interval (1000–3000) keV) was achieved by exploiting the anti-coincidence with the $CdWO_4$ counters. The background was significantly suppressed by the selection of events in the $^{106}CdWO_4$ detector in coincidence with the event(s) in at least one of the $CdWO_4$ counters with the energy release $E = 511 \pm 2\sigma$ keV (by a factor ∼17 in the same energy interval; here, σ is the energy resolution of the $CdWO_4$ counters for 511 keV γ quanta), and by selection of events in coincidence with the events in both the $CdWO_4$ counters with the energy $E = 511 \pm 2\sigma$ keV (by a further factor ∼42). Figure 6 presents the stages of the background spectra reduction.

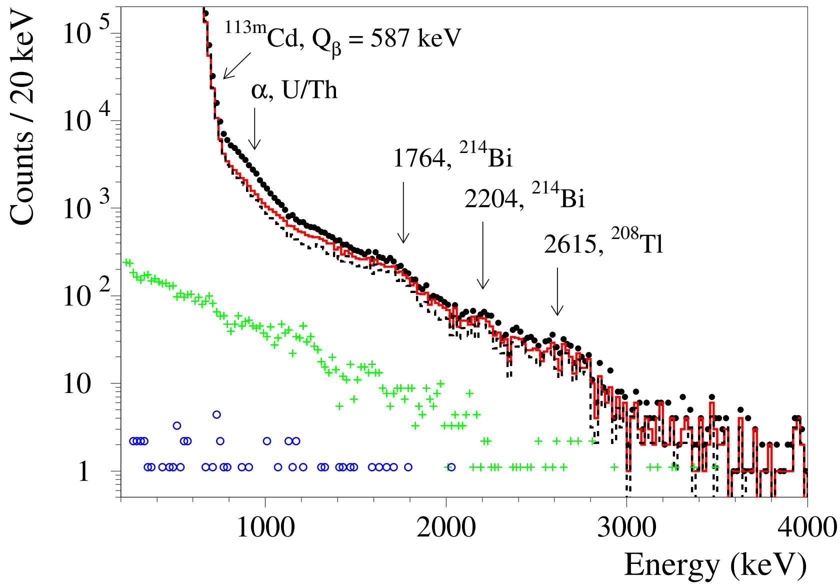

Figure 6. Energy spectra measured by the $^{106}CdWO_4$ detector for 26,033 h in the low-background set-up without selection cuts (black dots), after selection of γ and β events by PSD using the mean time method (solid red line), the γ and β events in anti-coincidence with the $CdWO_4$ counters (dashed black line), the γ and β events in coincidence with event(s) in at least one of the $CdWO_4$ counters with the energy $E = 511 \pm 2\sigma$ keV (green crosses), the γ, and β events in coincidence with events in both the $CdWO_4$ counters with the energy $E = 511 \pm 2\sigma$ keV (blue circles).

The counting rate of the $^{106}CdWO_4$ detector below the energy of ∼0.8 MeV is mainly caused by the β decay of ^{113}Cd with the energy $Q_\beta = 323.83(27)$ keV [22] and of ^{113m}Cd ($Q_\beta = 587.37(27)$ keV [22,41]). A background model to describe the experimental data after the ^{113m}Cd β spectrum was constructed from distributions of "internal" (radioactive contamination of the $^{106}CdWO_4$ crystal) and "external" (radioactive contamination of the set-up details) sources. The equilibrium of the ^{238}U and ^{232}Th chains in all the materials is assumed to be broken[1]. The sub-chains ^{228}Ra→^{228}Th, ^{228}Th→^{208}Pb (the ^{232}Th family) and ^{238}U→^{234}U, ^{226}Ra→^{210}Pb, ^{210}Pb→^{206}Pb (^{238}U) were assumed to be in secular equilibrium.

The following "internal" sources were simulated in the $^{106}CdWO_4$ crystal scintillator:

- ^{40}K, ^{228}Ra→^{228}Th, ^{228}Th→^{208}Pb, ^{226}Ra→^{210}Pb, and ^{210}Pb→^{206}Pb with activities estimated in the earlier stages of the experiment [45,46];
- distribution of α particles of ^{232}Th and ^{238}U with their daughters not discarded by the pulse-shape analysis; and,
- two-neutrino double beta decay of ^{116}Cd with the half-life $T_{1/2} = 2.63 \times 10^{19}$ yr [47].

The following "external" sources were simulated in the materials of the set-up:

1 Secular equilibrium in the ^{232}Th and ^{238}U decay families (when activities of daughter nuclides are equal to the activity of their parent nuclide) is typically broken in almost all of the materials due to physical or chemical processes utilized in the material production (see, e.g., [42–44]).

- ^{40}K, ^{228}Ra→^{228}Th, ^{228}Th→^{208}Pb, ^{226}Ra→^{210}Pb in the internal and external copper details, the quartz light guides, the $PbWO_4$ crystal light-guide, the PMTs;
- ^{210}Pb→^{206}Pb in the $PbWO_4$ crystal light-guide;
- ^{228}Th→^{208}Pb and ^{226}Ra→^{210}Pb in the $CdWO_4$ crystal scintillators; and,
- ^{56}Co and ^{60}Co in the internal copper bricks.

The background components were simulated using the EGSnrc package with initial kinematics given by the DECAY0 event generator [48]. The distribution of residual α particles of ^{232}Th and ^{238}U with their daughters was constructed from the experimental data using the pulse-shape analysis.

The simulated models were used to fit the energy spectra of γ and β events in anti-coincidence with the $CdWO_4$ counters and in coincidence with event(s) in at least one of the $CdWO_4$ counters with the energy release $E = 511 \pm 2\sigma$ keV. The data were fitted in the energy intervals (940–4000) keV (anti-coincidence data) and (240–3940) keV (coincidence with 511 keV). The fit quality is reasonable ($\chi^2 = 457$ for 235 degrees of freedom). Figure 7 shows the results of the fit and the main components of the background.

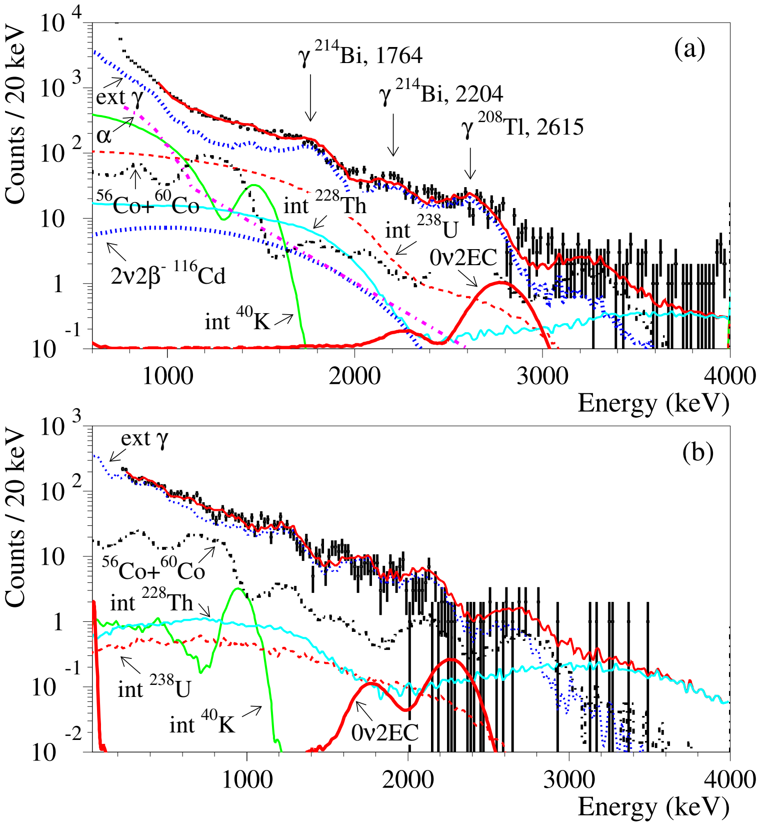

Figure 7. Energy spectra of the γ and β events accumulated for 26,033 h by the $^{106}CdWO_4$ scintillation detector in anti-coincidence with the $CdWO_4$ counters (**a**) and in coincidence with the 511 keV annihilation γ quanta in at least one of the $CdWO_4$ counters (**b**) (points) together with the background model (red line). The main components of the background are shown: the distributions of internal contaminations ("int ^{40}K", "int ^{232}Th", and "int ^{238}U") and external γ quanta ("ext γ"), residual α particles in the $^{106}CdWO_4$ crystal (α), cosmogenic ^{56}Co and ^{60}Co in the copper shield details, and the $2\nu2\beta$ decay of ^{116}Cd. The excluded distributions of the 0ν2EC decay of ^{106}Cd to the ground state of ^{106}Pd with the half-life $T_{1/2} = 6.8 \times 10^{20}$ yr are shown by red solid line.

The fit allowed to estimate limits on radioactive contamination of the materials of the low-background set-up. Table 1 presents the data.

Table 1. Radioactive contamination (mBq/kg) of the materials of the low-background set-up estimated by using the fit of the energy spectra that are presented in Figure 7. Upper limits are given at 68% C.L.

Material	^{40}**K**	^{56}**Co**	^{60}**Co**	^{88}**Y**	^{210}**Pb**	^{226}**Ra**	^{228}**Ac**	^{228}**Th**
$PbWO_4$ crystal	$\leq$0.09	–	–	–	$\leq 12 \times 10^3$	$\leq$ 0.07	$\leq$0.28	$\leq$0.23
$CdWO_4$ crystals	–	–	–	–	–	$\leq$0.27	–	$\leq$0.014
Quartz light-guides	$\leq$18	–	–	–	–	$\leq$3.3	$\leq$0.6	$\leq$0.6
Copper internal	$\leq$0.8	$\leq$0.26	$\leq$0.5	$\leq$0.005	–	$\leq$3.0	$\leq$1.3	$\leq$0.019
Copper external	$\leq$1.4	–	–	–	–	$\leq$1.5	$\leq$3.2	$\leq$0.026
PMTs	$\leq$1060	–	–	–	–	$\leq$140	$\leq$1030	$\leq$250

3.2. Limits on 2EC, ECβ^+ and 2β^+ Processes in ^{106}Cd

There are no peculiarities in the experimental data that could be ascribed to 2β processes in ^{106}Cd. Lower limits on the half-life of ^{106}Cd relatively to different 2β decay channels and modes can be estimated using the following formula:

$$\lim T_{1/2} = N \cdot \ln 2 \cdot \eta_{\rm det} \cdot \eta_{\rm sel} \cdot t / \lim S, \quad (2)$$

where N is the number of ^{106}Cd nuclei in the $^{106}CdWO_4$ crystal (2.42×10^{23}), $\eta_{\rm det}$ is the detection efficiency for the process of decay (calculated as a ratio of the events number in a simulated distribution to the number of generated events), $\eta_{\rm sel}$ is the selection cuts efficiency (selection by PSD, time coincidence, energy interval), t is the time of measurements, and $\lim S$ is the number of events of the effect searched for, which can be excluded at a given confidence level (C.L.). The responses of the detector system to different modes and channels of ^{106}Cd double beta decay were simulated while using the EGSnrc package with initial kinematics that were given by the DECAY0 event generator. Approximately 5×10^6 events were generated for each decay channel.

Different data were analyzed in order to estimate limits on the 2β processes in ^{106}Cd. Fit of the anti-coincidence spectrum by the above described model plus a simulated distribution of the 0ν2EC decay of ^{106}Cd to the ground state of ^{106}Pd returns the area of the distribution (205 ± 99) counts that is no evidence for the effect searched for. According to [49], we took 367 events as $\lim S$ at 90% C.L.[2] The detection efficiency for the decay was simulated as $\eta_{\rm det} = 0.522$. Taking into account the selection cut efficiency due to application of the PSD to select γ and β events $\eta_{\rm sel} = 0.955$, we got a lower limit on the half-life of ^{106}Cd relative to the 0ν2EC decay to the ground state of ^{106}Pd $T_{1/2} \geq 6.8 \times 10^{20}$ yr (the excluded distribution of the 0ν2EC decay is shown in Figure 7). The limit is slightly worse than the one that was obtained in the previous stage of the experiment ($T_{1/2} \geq 1.0 \times 10^{21}$ yr [21], also see Table 2).

Fit of the $^{106}CdWO_4$ detector data in coincidence with signal(s) in the $CdWO_4$ counters by the above described background model was more sensitive to the most of the modes and channels of the decay searched for. An example of such an analysis for the 0νECβ^+ and 0ν2β^+ decays of ^{106}Cd to the ground state of ^{106}Pd using the data that were measured with the $^{106}CdWO_4$ detector in coincidence with 511 keV events in at least one of the $CdWO_4$ counters is shown in Figure 8. The selection cuts efficiency, e.g., for the 0νECβ^+ process was calculated to be $\eta_{\rm sel} = 0.909$ as a product of the PSD to select γ and β events in the interval $\pm 2\sigma$ of the mean time values (0.9546), the time coincidence efficiency in the interval $\pm 3\sigma$ (0.9973), and the energy interval $\pm 2\sigma$ to select 511 keV events in the $CdWO_4$ counters (0.9545). Table 2 provides the data on the efficiencies, values of $\lim S$, and the obtained half-life limits.

[2] In the present work all the limits are given with 90% C.L. Only statistical errors coming from the data fluctuations were taken into account in the estimations of the $\lim S$ values, and systematic contributions have not been included in the half-life limit values.

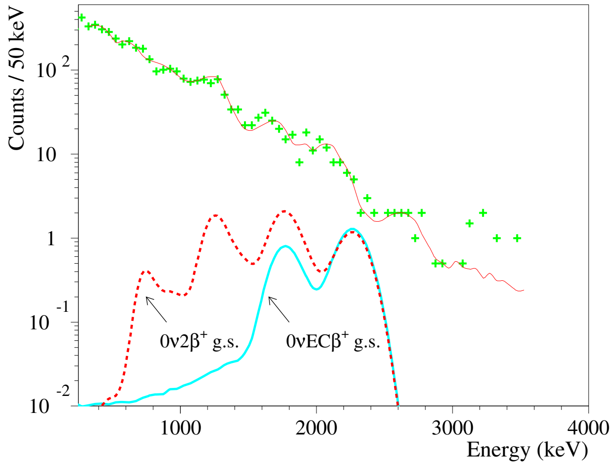

Figure 8. Energy spectrum of the γ and β events measured for 26,033 h by the $^{106}CdWO_4$ detector in coincidence with events in at least one of the $CdWO_4$ counters with energy $E = 511 \pm 2\sigma$ keV (crosses). The solid red line shows the fit of the data by the background model (see Section 3.1). Excluded distributions of $0\nu EC\beta^+$ and $0\nu 2\beta^+$ decays of ^{106}Cd to the ground state of ^{106}Pd with the half-lives $T_{1/2} = 1.4 \times 10^{22}$ yr and $T_{1/2} = 5.9 \times 10^{21}$ yr, respectively, are shown.

Another example is the search for 0ν2EC transition of ^{106}Cd to the 2718 keV excited level of ^{106}Pd (considered as one of the most promising decay channels from the point of view of a possible resonant process [14]). The search was realized by analysis of the $^{106}CdWO_4$ detector data in coincidence with event(s) in at least one of the $CdWO_4$ counters in the energy interval $(1046 - 1.5\sigma) - (1160 + 1.7\sigma)$ keV. The interval should contain two intensive γ quanta with energies 1046 keV and 1160 keV being expected in the decay searched for (see the decay scheme in Figure 1). Figure 9 presents the spectrum and its fit, consisting of the background model and excluded distribution of the resonant process searched for.

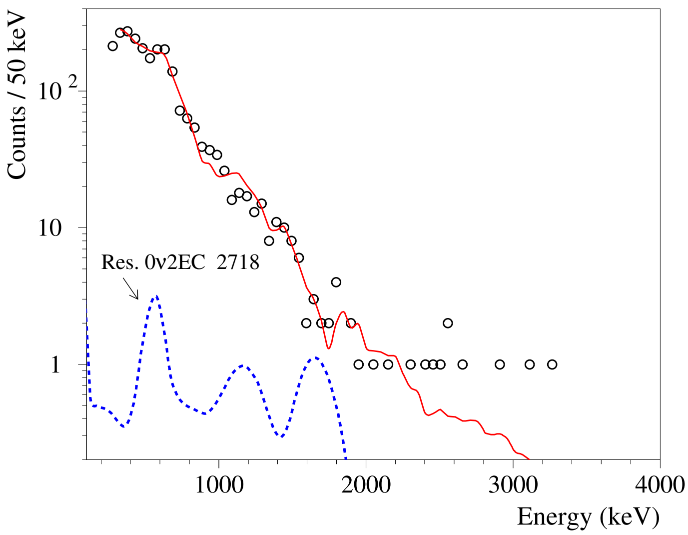

Figure 9. Energy spectrum of γ and β events measured by the $^{106}CdWO_4$ detector for 26,033 h in coincidence with event(s) in at least one of the $CdWO_4$ counters in the energy interval $(1046 - 1.5\sigma)$ – $(1160 + 1.7\sigma)$ keV (circles) and its fit by the model of background (red line). The excluded distribution of a possible resonant 0ν2EC decay of ^{106}Cd to the 2718 keV excited level of ^{106}Pd with the half-life $T_{1/2} = 2.9 \times 10^{21}$ yr is shown.

The highest sensitivity to several decay channels with positron(s) emission was achieved using the data that were gathered by the $^{106}CdWO_4$ detector in coincidence with 511 keV annihilation γ quanta in both of the $CdWO_4$ counters thanks to a rather high detection efficiency of the $CdWO_4$

counters and a very low background counting rate (see Figure 10). However, the fit of the spectrum by the background components is not reliable enough, due to the very low statistics of the data. Thus, the method of comparison of the measured background with the expected one was applied for the analysis. The expected background was estimated from the results of the fit that is shown in Figure 7. There are 54 counts in the whole spectrum, while the estimated background is 55.3 counts, confirming a correct background modelling. In the energy interval (250–1000) keV, the measured background is 33 counts, while the estimated one is 37.4 counts that leads to $\lim S = 6.7$ counts in accordance with the recommendations [49]. Taking into account the detection and the selections efficiencies for the $2\nu EC\beta^+$ decay of ^{106}Cd to the ground state of ^{106}Pd (0.040 and 0.703, respectively), one can obtain a half-life limit $T_{1/2} = 2.1 \times 10^{21}$ yr that is about two times higher than the limit ($T_{1/2} = 1.1 \times 10^{21}$ yr) that was obtained in the previous stage of the experiment [34].

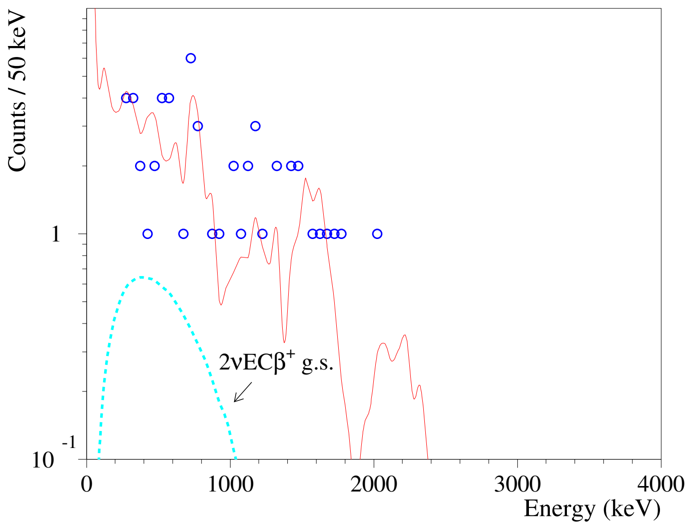

Figure 10. Energy spectrum of γ and β events measured by the $^{106}CdWO_4$ detector for 26,033 h in coincidence with 511 keV annihilation γ quanta in both of the $CdWO_4$ counters (circles). The expected background, which was built on the basis of the fit presented in Figure 7, is shown by a red solid line. The excluded distribution of the $2\nu EC\beta^+$ decay of ^{106}Cd to the ground state of ^{106}Pd with the half-life $T_{1/2} = 2.1 \times 10^{21}$ yr is shown.

Limits on other 2β decay processes in ^{106}Cd were obtained in a similar way. They are presented in Table 2, where the results of the most sensitive previous experiments are given for comparison.

A limit on effective nuclear matrix elements for the $2\nu EC\beta^+$ decay of ^{106}Cd to the ground state of ^{106}Pd could be estimated using the calculations of the phase-space factors for the decay [50,51] with the formula $1/T_{1/2} = G^{2\nu EC\beta^+} \times |M^{eff}|^2$. The effective matrix nuclear element M^{eff} is expressed by $M^{eff} = g_A^2 \times M^{2\nu EC\beta^+}$, where g_A is the axial-vector coupling constant, $M^{2\nu EC\beta^+}$ is nuclear matrix element. An upper limit on the value of the effective matrix nuclear element for the process can be estimated as $M^{eff} \leq$ (0.80–0.82).

The half-life limit on the $2\nu EC\beta^+$ decay of ^{106}Cd to the ground state of ^{106}Pd, $T_{1/2} \geq 2.1 \times 10^{21}$ yr, approaches the region of the theoretical predictions that are in the range 10^{21}–10^{22} yr [10,52–55]. The sensitivity to the double beta decay processes presented in ^{106}Cd is expected to be improved in the currently running experiment with reduced background thanks to the utilization of ultra-radiopure PMTs, longer quartz light-guides for the $CdWO_4$ counters, a more powerful passive shield of the detector system. Additionally, the energy resolution of the $^{106}CdWO_4$ detector was improved, roughly by a factor $\sim$1.8, thanks to the replacement of the $PbWO_4$ light-guide by a plastic scintillator light-guide with substantially better optical transmittance. This replacement became possible due to an extremely low radioactive contamination of the specially developed R11065-20 MOD Hamamatsu PMT [56] used for the $^{106}CdWO_4$ detector.

Table 2. Half-life limits on 2β processes in ^{106}Cd. The experimental selection is also reported (AC, anti-coincidence; CC, in coincidence, at the given energy (energies) with $CdWO_4$; CC 511&511, in coincidence with energies 511 keV in both of the $CdWO_4$ counters). η_{det} denotes the detection efficiency, η_{sel} is the selection cuts efficiency. The results of the most sensitive previous experiments are given for comparison.

Decay,	Exp.	η_{det}	η_{sel}	lim S	lim $T_{1/2}$ (yr) at 90% C.L.	
Level of ^{106}Pd	Selection				Present Work	Best Previous
2ν2EC 2^+ 1128	CC 616	0.135	0.909	92	$\geq 6.6 \times 10^{20}$	$\geq 5.5 \times 10^{20}$ [34]
2ν2EC 0^+ 1134	CC 622	0.188	0.909	86	$\geq 9.9 \times 10^{20}$	$\geq 1.0 \times 10^{21}$ [34]
2ν2EC 2^+ 1562	CC 1050	0.138	0.909	80	$\geq 7.8 \times 10^{20}$	$\geq 7.4 \times 10^{20}$ [34]
2ν2EC 0^+ 1706	CC 1194	0.134	0.909	90	$\geq 6.7 \times 10^{20}$	$\geq 7.1 \times 10^{20}$ [34]
2ν2EC 0^+ 2001	CC 873	0.153	0.909	46	$\geq 1.5 \times 10^{21}$	$\geq 9.7 \times 10^{20}$ [34]
2ν2EC 0^+ 2278	CC 1766	0.091	0.909	131	$\geq 3.1 \times 10^{20}$	$\geq 1.0 \times 10^{21}$ [34]
0ν2EC g.s.	AC	0.522	0.955	367	$\geq 6.8 \times 10^{20}$	$\geq 1.0 \times 10^{21}$ [21]
0ν2EC 2^+ 512	AC	0.319	0.955	443	$\geq 3.4 \times 10^{20}$	$\geq 5.1 \times 10^{20}$ [21]
0ν2EC 2^+ 1128	CC 616	0.118	0.909	110	$\geq 4.9 \times 10^{20}$	$\geq 5.1 \times 10^{20}$ [34]
0ν2EC 0^+ 1134	CC 622	0.155	0.909	109	$\geq 6.4 \times 10^{20}$	$\geq 1.1 \times 10^{21}$ [34]
0ν2EC 2^+ 1562	CC 1050	0.136	0.909	45	$\geq 1.4 \times 10^{21}$	$\geq 7.3 \times 10^{20}$ [34]
0ν2EC 0^+ 1706	CC 1194	0.120	0.909	27	$\geq 2.0 \times 10^{21}$	$\geq 1.0 \times 10^{21}$ [34]
0ν2EC 0^+ 2001	CC 873	0.135	0.909	177	$\geq 3.5 \times 10^{20}$	$\geq 1.2 \times 10^{21}$ [34]
0ν2EC 0^+ 2278	CC 1766	0.079	0.909	29	$\geq 1.2 \times 10^{21}$	$\geq 8.6 \times 10^{20}$ [34]
Res. 0ν2K 2718	CC 1046 + 1160	0.215	0.909	33	$\geq 2.9 \times 10^{21}$	$\geq 1.1 \times 10^{21}$ [34]
Res. $0\nu KL_1$ 4^+ 2741	AC	0.454	0.952	663	$\geq 3.2 \times 10^{20}$	$\geq 9.5 \times 10^{20}$ [21]
Res. $0\nu KL_3$ $2,3^-$ 2748	AC	0.318	0.955	432	$\geq 3.5 \times 10^{20}$	$\geq 1.4 \times 10^{21}$ [34]
2νECβ^+ g.s.	CC 511&511	0.040	0.703	6.7	$\geq 2.1 \times 10^{21}$	$\geq 1.1 \times 10^{21}$ [34]
2νECβ^+ 2^+ 512	CC 511&511	0.047	0.459	4.0	$\geq 2.7 \times 10^{21}$	$\geq 1.3 \times 10^{21}$ [34]
2νECβ^+ 2^+ 1128	CC 511&511	0.029	0.509	5.6	$\geq 1.3 \times 10^{21}$	$\geq 1.0 \times 10^{21}$ [34]
2νECβ^+ 0^+ 1134	CC 511&511	0.031	0.603	11	$\geq 8.5 \times 10^{20}$	$\geq 1.1 \times 10^{21}$ [34]
0νECβ^+ g.s.	CC 511	0.376	0.909	12	$\geq 1.4 \times 10^{22}$	$\geq 2.2 \times 10^{21}$ [21]
0νECβ^+ 2^+ 512	CC 511	0.384	0.909	18	$\geq 9.7 \times 10^{21}$	$\geq 1.9 \times 10^{21}$ [34]
0νECβ^+ 2^+ 1128	CC 511	0.314	0.909	14	$\geq 1.0 \times 10^{22}$	$\geq 1.3 \times 10^{21}$ [34]
0νECβ^+ 0^+ 1134	CC 511&511	0.030	0.385	5.0	$\geq 1.2 \times 10^{21}$	$\geq 1.9 \times 10^{21}$ [34]
$2\nu 2\beta^+$ g.s.	CC 511&511	0.052	0.385	5.8	$\geq 1.7 \times 10^{21}$	$\geq 2.3 \times 10^{21}$ [34]
$2\nu 2\beta^+$ 2^+ 512	CC 511&511	0.048	0.323	3.4	$\geq 2.3 \times 10^{21}$	$\geq 2.5 \times 10^{21}$ [34]
$0\nu 2\beta^+$ g.s.	CC 511	0.391	0.909	30	$\geq 5.9 \times 10^{21}$	$\geq 3.0 \times 10^{21}$ [34]
$0\nu 2\beta^+$ 2^+ 512	CC 511	0.370	0.909	39	$\geq 4.0 \times 10^{21}$	$\geq 2.5 \times 10^{21}$ [34]

4. Conclusions

The experiment to search for double beta decay of ^{106}Cd with enriched $^{106}CdWO_4$ scintillator in coincidence with two large volume $CdWO_4$ scintillation counters was performed at the Gran Sasso underground laboratory of INFN (Italy). New improved limits are set on the different channels of ^{106}Cd double beta decay at the level of $10^{20} - 10^{22}$ yr. The new improved limit on half-life of ^{106}Cd relative to the 2νECβ^+ decay was estimated as $T_{1/2} \geq 2.1 \times 10^{21}$ yr. The sensitivity is within the region of the theoretical predictions for the decay probability that are in the range of $T_{1/2} \sim 10^{21} - 10^{22}$ yr. A new improved limit was set for the resonant neutrinoless double-electron capture to the 2718 keV excited level of ^{106}Pd, as $T_{1/2}^{0\nu 2K} \geq 2.9 \times 10^{21}$ yr.

The next stage of experiment is running at LNGS in the DAMA/R&D set-up with an improved sensitivity to all of the decay channels, thanks to a reduction of the background approximately by a factor 3–5 with utilization of ultra-radiopure PMTs, longer quartz light-guides for the $CdWO_4$ counters, and a more powerful passive shield of the detector system. The energy resolution of the $^{106}CdWO_4$ detector was also improved thanks to replacement of the $PbWO_4$ light-guide by a plastic scintillator light-guide with a substantially better optical transmittance. As a result, the sensitivity to the $2\nu EC\beta^+$ decay of ^{106}Cd is expected to be high enough to detect the process with the half-life at level of $\sim(0.5-1)\times10^{22}$ yr over five yr of measurements.

Author Contributions: All the authors of this paper have been significantly contributing to the presented results working on the various aspects of the different phases of this experiment. All authors have read and agreed to the published version of the manuscript.

Funding: This research received no external funding.

Acknowledgments: D.V.K. and O.G.P. were supported in part by the project "Investigation of double beta decay, rare alpha and beta decays" of the program of the National Academy of Sciences of Ukraine "Laboratory of young scientists" Grant No. 0120U101838. F.A.D., D.V.K., V.R.K., V.V.K., V.I.T. and M.M.Z. were supported in part by the project "Double beta decay" of the National Research Foundation of Ukraine Grant No. 2020.02/0011. F.A.D. greatly acknowledges the Government of Ukraine for the quarantine measures that have been taken against the Coronavirus disease 2019 that substantially reduced much unnecessary bureaucratic work.

Conflicts of Interest: The authors declare no conflict of interest.

References

1. Giuliani, A.; Poves, A. Neutrinoless Double-Beta Decay. *AHEP* **2012**, *2012*, 857016. [CrossRef]
2. Cremonesi, O.; Pavan, M. Challenges in Double Beta Decay. *AHEP* **2014**, *2014*, 951432. [CrossRef]
3. Vergados, J.D.; Ejiri, H.; Šimkovic, F. Neutrinoless double beta decay and neutrino mass. *Int. J. Mod. Phys. E* **2016**, *25*, 1630007. [CrossRef]
4. Bilenky, S.M.; Giunti, C. Neutrinoless double-beta decay: A probe of physics beyond the Standard Model. *Int. J. Mod. Phys. A* **2015**, *30*, 1530001. [CrossRef]
5. Dell'Oro, S.; Marcocci, S.; Viel, M.; Vissani, F. Neutrinoless Double Beta Decay: 2015 Review. *AHEP* **2016**, *2016*, 2162659. [CrossRef]
6. Dolinski, M.J.; Poon, A.W.P.; Rodejohann, W. Neutrinoless double beta decay: Status and prospects. *Annu. Rev. Nucl. Part. Sci.* **2019**, *69*, 219–251. [CrossRef]
7. Asaka, T.; Shaposhnikov, M. The νMSM, dark matter and baryon asymmetry of the universe. *Phys. Lett. B* **2005**, *620*, 17–26. [CrossRef]
8. Deppisch, F.F.; Graf, L.; Harz, J.; Huang, W.C. Neutrinoless double beta decay and the baryon asymmetry of the Universe. *Phys. Rev. D* **2018**, *98*, 055029. [CrossRef]
9. Barabash, A.S. Precise Half-Life Values for Two-Neutrino Double-β Decay: 2020 Review. *Universe* **2020**, *6*, 159. [CrossRef]
10. Hirsch, M.; Muto, K.; Oda, T.; Klapdor-Kleingrothaus, H.V. Nuclear structure calculation of $\beta^+\beta^+$, β^+EC, and EC/EC decay matrix elements. *Z. Phys. A* **1994**, *347*, 151–160. [CrossRef]
11. Winter, R. Double K capture and single K capture with positron emission. *Phys. Rev.* **1955**, *100*, 142–144. [CrossRef]
12. Voloshin, M.B.; Mitselmakher, G.V.; Eramzhyan, R.A. Conversion of an atomic electron into a positron and double β^+ decay. *JETP Lett.* **1982**, *35*, 656–659.
13. Bernabeu, J.; De Rujula, A.; Jarlskog, C. Neutrinoless double electron capture as a tool to measure the electron neutrino mass. *Nucl. Phys. B* **1983**, *223*, 15–28. [CrossRef]
14. Krivoruchenko, M.I.; Šimkovic, F.; Frekers, D.; Faessler, F. Resonance enhancement of neutrinoless double electron capture. *Nucl. Phys. A* **2011**, *859*, 140–171. [CrossRef]
15. Meshik, A.P.; Hohenberg, C.M.; Pravdivtseva, O.V.; Kapusta, Y.S. Weak decay of ^{130}Ba and ^{132}Ba: Geochemical measurements. *Phys. Rev. C* **2001**, *64*, 035205. [CrossRef]
16. Pujol, M.; Marty, B.; Burnard, B.P.; Philippot, P. Xenon in Archean barite: Weak decay of ^{130}Ba, mass-dependent isotopic fractionation and implication for barite formation. *Geochim. Cosmochim. Acta* **2009**, *73*, 6834–6846. [CrossRef]

17. Meshik, A.; Pravdivtseva, O. Weak Decay of Tellurium and Barium Isotopes in Geological Samples: Current Status. *JPS Conf. Proc.* **2017**, *14*, 020702.
18. Gavrilyuk, Y.M.; Gangapshev, A.M.; Kazalov, V.V.; Kuzminov, V.V.; Panasenko, S.I.; Ratkevich S.S.; Indications of $2\nu 2K$ capture in ^{78}Kr. *Phys. Rev. C* **2013**, *87*, 035501. [CrossRef]
19. Ratkevich, S.S.; Gangapshev, A.M.; Gavrilyuk, Y.M.; Karpeshin, F.F.; Kazalov, V.V.; Kuzminov, V.V.; Panasenko, S.I.; Trzhaskovskaya, M.B.; Yakimenko, S.P. Comparative study of the double-K-shell-vacancy production in single- and double-electron-capture decay. *Phys. Rev. C* **2017**, *96*, 065502. [CrossRef]
20. XENON Collaboration. Observation of two-neutrino double electron capture in ^{124}Xe with XENON1T. *Nature* **2019**, *568*, 532–535. [CrossRef]
21. Belli, P.; Bernabei, R.; Boiko, R.S.; Brudanin, V.B.; Cappella, F.; Caracciolo, V.; Cerulli, R.; Chernyak, D.M.; Danevich, F.A.; d'Angelo, S.; et al. Search for double-β decay processes in ^{106}Cd with the help of a $^{106}CdWO_4$ crystal scintillator. *Phys. Rev. C* **2012**, *85*, 044610. [CrossRef]
22. Wang, M.; Audi, G.; Kondev, F.G.; Huang, W.J.; Naimi, S.; Xu, X. The AME2016 atomic mass evaluation. *Chin. Phys. C* **2017**, *41*, 030003. [CrossRef]
23. Meija, J.; Coplen, T.B.; Berglund, M.; Brand, W.A.; De Bièvre, P.; Gring, M.; Holden, N.E.; Irrgeher, J.; Loss, R.D.; Walczyk, T.; et al. Isotopic compositions of the elements 2013 (IUPAC Technical Report). *Pure Appl. Chem.* **2016**, *88*, 293–306. [CrossRef]
24. Kiel, H.; Münstermann, D.; Zuber, K. A search for various double beta decay modes of Cd, Te, and Zn isotopes. *Nucl. Phys. A* **2003**, *723*, 499–514. [CrossRef]
25. Ebert, J.; Fritts, M.; Gößling, C.; Göpfert, T.; Gehre, D.; Hagner, C.; Köttig, N.T.; Neddermann, T.; Oldorf, C.; Quante, T.; et al. Current status and future perspectives of the COBRA experiment. *Adv. High Energy Phys.* **2013**, *2013*, 703572. [CrossRef]
26. Ebert, J.; Fritts, M.; Gehre, D.; Gößling, C.; Hagner, C.; Heidrich, N.; Klingenberg, R.; Kröninger, K.; Nitsch, C.; Oldorf, C.; et al. Results of a search for neutrinoless double-β decay using the COBRA demonstrator. *Phys. Rev. C* **2016**, *94*, 024603. [CrossRef]
27. Rukhadze, N.I.; Briancon, C.; Brudanin, V.B.; Egorov, V.G.; Klimenko, A.A.; Kovalik, A.; Timkin, V.V.; Čhermák, P.; Shitov, Y.A.; Šimkovic, F.; et al. Search for double beta decay of ^{106}Cd. *Bull. Russ. Acad. Sci. Phys.* **2011**, *75*, 879–882. [CrossRef]
28. Rukhadze, N.I.; Bakalyarov, A.M.; Briançon, C.; Brudanin, V.B.; Cermák, P.; Egorov, V.G.; Klimenko, A.A.; Kovalík, A.; Lebedev, V.I.; Mamedov, F.; et al. New limits on double beta decay of ^{106}Cd. *Nucl. Phys. A* **2011**, *852*, 197–206. [CrossRef]
29. Rukhadze, N.I.; Beneš, P.; Briançon, C.; Brudanin, V.B.; Cermák, P.; Danevich, F.A.; Egorov, V.G.; Gusev, K.N.; Klimenko, A.A.; Kovalenko, V.E.; et al. Search for double electron capture of ^{106}Cd. *Phys. At. Nucl.* **2006**, *69*, 2117–2123. [CrossRef]
30. Rukhadze, N.I.; Brudanin, V.B.; Egorov, V.G.; Klimenko, A.A.; Kovalik, A.; Kouba, P.; Piquemal, F.; Rozov, S.V.; Rukhadze, E.; Salamatin, A.V.; et al. Search for double beta decay of ^{106}Cd in the TGV-2 experiment. *J. Phys. Conf. Ser.* **2016**, *718*, 062049. [CrossRef]
31. Rukhadze, N.; on behalf of TGV Collaboration. Search for double beta decay of ^{106}Cd with the TGV-2 spectrometer. *PoS* **2016**, *281*, 245.
32. Belli, P.; Bernabei, R.; Boiko, R.S.; Brudanin, V.B.; Bukilic, N.; Cerulli, R.; Chernyak, D.M.; Danevich, F.A.; d'Angelo, S.; Dossovitskiy, A.E.; et al. Development of enriched $^{106}CdWO_4$ crystal scintillators to search for double β decay processes in ^{106}Cd. *Nucl. Instrum. Meth. A* **2010**, *615*, 301–306. [CrossRef]
33. Laubenstein, M.; Hult, M.; Gasparro, J.; Arnold, D.; Neumaier, S.; Heusser, G.; Köhler, M.; Povinec, P.; Reyss, J.-L.; Schwaiger, M.; Theodórsson, P. Underground measurements of radioactivity. *Appl. Radiat. Isot.* **2004**, *61*, 167. [CrossRef] [PubMed]
34. Belli, P.; Bernabei, R.; Brudanin, V.B.; Cappella, F.; Caracciolo, V.; Cerulli, R.; Chernyak, D.M.; Danevich, F.A.; d'Angelo, S.; Di Marco, A.; et al. Search for double-β decay in ^{106}Cd with an enriched $^{106}CdWO_4$ crystal scintillator in coincidence with four HPGe detectors. *Phys. Rev. C* **2016**, *93*, 045502. [CrossRef]
35. Polischuk, O.G.; Belli, P.; Bernabei, R.; Brudanin, V.B.; Cappella, F.; Caracciolo, V.; Cerulli, R.; Danevich, F.A.; Incicchitti, A.; Kasperovych, D.V.; et al. New limit on two neutrino electron capture with positron emission in ^{106}Cd. *AIP Conf. Proc.* **2019**, *2165*, 020020.
36. De Frenne, D.; Negret, A. Nuclear data sheets for A = 106. *Nucl. Data Sheets* **2008**, *109*, 943–1102. [CrossRef]

37. Boiko, R.S.; Virich, V.D.; Danevich, F.A.; Dovbush, T.I.; Kovtun, G.P.; Nagornyi, S.S.; Nisi, S.; Samchuk, A.I.; Solopikhin, D.A.; Shcherban, A.P. Ultrapurification of archaeological lead. *Inorg. Mater.* **2011**, *47*, 645–648. [CrossRef]
38. Danevich, F.A.; Kim, S.K.; Kim, H.J.; Kim, Y.D.; Kobychev, V.V.; Kostezh, A.B.; Kropivyansky, B.N.; Laubenstein, M.; Mokina, V.M.; Nagorny, S.S.; et al. Ancient Greek lead findings in Ukraine. *Nucl. Instr. Meth. A* **2009**, *603*, 328–332. [CrossRef]
39. Bernabei, R.; Belli, P.; Cappella, F.; Cerulli, R.; Dai, C.J.; d'Angelo, A.; He, H.L.; Incicchitti, A.; Kuang, H.H.; Ma, J.M.; et al. First results from DAMA/LIBRA and the combined results with DAMA/NaI. *Eur. Phys. J. C* **2008**, *56*, 333–355. [CrossRef]
40. Kawrakow, I.; Rogers, D.W.O. *The EGSnrc Code System: Monte Carlo Simulation of Electron and Photon Transport, NRCC Report PIRS-701*; National Research Council of Canada: Ottawa, ON, USA, 2003.
41. Blachot, J. Nuclear data sheets for A = 113. *Nucl. Data Sheets* **2010**, *111*, 1471–1618. [CrossRef]
42. Jagam, P.; Simpson, J.J. Measurements of Th, U and K concentrations in a variety of materials. *Nucl. Instr. Meth. A* **1993**, *324*, 389–398. [CrossRef]
43. Righi, S.; Betti, M.; Bruzzi, L.; Mazzotti, G. Monitoring of natural radioactivity in working places. *Microchem. J.* **2000**, *67*, 119–126. [CrossRef]
44. Danevich, F.A.; Tretyak, V.I. Radioactive contamination of scintillators. *Int. J. Mod. Phys. A* **2018**, *33*, 1843007. [CrossRef]
45. Danevich, F.A.; Barabash, A.S.; Belli, P.; Bernabei, R.; Boiko, R.S.; Brudanin, V.B.; Cappella, F.; Caracciolo, V.; Cerulli, R.; Chernyak, D.M.; et al. Development of radiopure cadmium tungstate crystal scintillators from enriched ^{106}Cd and ^{116}Cd to search for double beta decay. *AIP Conf. Proc.* **2013**, *1549*, 201–204.
46. Poda, D.V.; Barabash, A.S.; Belli, P.; Bernabei, R.; Boiko, R.S.; Brudanin, V.B.; Cappella, F.; Caracciolo, V.; Castellano, S.; Cerulli, R.; et al. $CdWO_4$ crystal scintillators from enriched isotopes for double beta decay experiments. *Radiat. Meas.* **2013**, *56*, 66–69. [CrossRef]
47. Barabash, A.S.; Belli, P.; Bernabei, R.; Cappella, F.; Caracciolo, V.; Cerulli, R.; Chernyak, D.M.; Danevich, F.A.; d'Angelo, A.; Incicchitti, A.; et al. Final results of the Aurora experiment to study 2β decay of ^{116}Cd with enriched $^{116}CdWO_4$ crystal scintillators. *Phys. Rev. D* **2018**, *98*, 092007. [CrossRef]
48. Ponkratenko, O.A.; Tretyak, V.I.; Zdesenko, Y.G. Event generator DECAY4 for simulation of double-beta processes and decays of radioactive nuclei. *Phys. Atom. Nucl.* **2000**, *63*, 1282–1287. [CrossRef]
49. Feldman, G.J.; Cousins, R.D. Unified approach to the classical statistical analysis of small signals. *Phys. Rev. D* **1998**, *57*, 3873–3889. [CrossRef]
50. Kotila, J.; Iachello, F. Phase space factors for $\beta^+\beta^+$ decay and competing modes of double-β decay. *Phys. Rev. C* **2013**, *87*, 024313. [CrossRef]
51. Mirea, M.; Pahomi, T.; Stoica, S. Values of the phase space factors involved in double beta decay. *Rom. Rep. Phys.* **2015**, *67*, 872–889.
52. Barabash, A.S.; Umatov, V.I.; Gurriarán, R.; Hubert, F.; Hubert, P.; Aunola, M.; Suhonen, J. Theoretical and experimental investigation of the double beta processes in ^{106}Cd. *Nucl. Phys. A* **1996**, *604*, 115–128. [CrossRef]
53. Toivanen, J.; Suhonen, J. Study of several double-β-decaying nuclei using the renormalized proton-neutron quasiparticle random-phase approximation. *Phys. Rev. C* **1997**, *55*, 2314–2323. [CrossRef]
54. Rumyantsev, O.A.; Urin, M.H. The strength of the analog and Gamow-Teller giant resonances and hindrance of the $2\nu\beta\beta$-decay rate. *Phys. Lett. B* **1998**, *443*, 51–57. [CrossRef]
55. Ejiri, H. Fermi surface quasi particle model nuclear matrix elements for two neutrino double beta decays. *J. Phys. G* **2017**, *44*, 115201. [CrossRef]
56. Bernabei, R.; Belli, P.; Bussolotti, A.; Cappella, F.; Caracciolo, V.; Casalboni, M.; Cerulli, R.; Dai, C.J.; d'Angelo, A.; Di Marco A.; et al. Performances of the new high quantum efficiency PMTs in DAMA/LIBRA. *JINST* **2012**, *7*, 03009. [CrossRef]

Publisher's Note: MDPI stays neutral with regard to jurisdictional claims in published maps and institutional affiliations.

© 2020 by the authors. Licensee MDPI, Basel, Switzerland. This article is an open access article distributed under the terms and conditions of the Creative Commons Attribution (CC BY) license (http://creativecommons.org/licenses/by/4.0/).